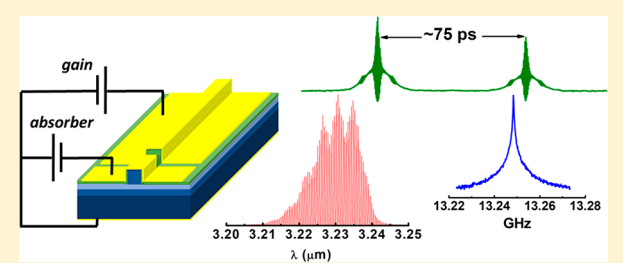


Passive Mode-Locking of 3.25 μ m GaSb-Based Cascade Diode Lasers

Tao Feng,[†] Leon Shterengas,*^{*,†} Takashi Hosoda,[†] Alexey Belyanin,[‡] and Gela Kipshidze[†]

ABSTRACT: Passively mode-locked type-I quantum well cascade diode lasers emitting near 3.25 µm were designed, fabricated, and characterized. The deep etched \sim 5.5- μ m-wide single spatial mode ridge waveguide design utilizing split-contact architecture was implemented. The epi-side-up mounted 3-mm-long ridge lasers with both 2.7-mm-long gain and 300-μm-long absorber sections forward biased operated in the continuous wave regime with above 12 mW of output power at 20 °C. The devices with a reversebiased absorber section generated ~10 ps pulses at the repetition rate of ~13.2 GHz with average power exceeding 1 mW. The laser



emission spectrum in the mode-locked regime comprised a smooth bell-shape-like frequency comb covering about a 20 nm range at the full-width at half-maximum level. Second-order interferometric autocorrelation studies revealed a strong spectral chirp in the pulse. The intermodal beat note of the Lorentzian shape with a 180 kHz line width was observed, corresponding to pulse-to-pulse timing jitter of about 110 fs/cycle. The small degree of the phase-locking was observed in autocorrelation scans even without reverse bias applied to the absorber section. The mapping of the radio frequency spectrum over variable gain and absorber section biases showed switching between two bistable mode-locking regimes at low absorber bias section voltages.

KEYWORDS: mode-locked, infrared, cascade laser, frequency comb, ultrafast laser, two-photon absorption

fter more than a decade of intense research on phase-Acoherent and mode-locked regimes of mid-infrared intersubband quantum cascade lasers (QCLs) there is now a consensus that passive mode-locking is impossible in these devices. The fundamental obstacle is an ultrafast gain relaxation time on the order of 1 ps, much shorter than the cavity round-trip time, which prevents the formation of isolated pulses. The only successful route to mode-locked pulses in QCLs turned out to be active mode-locking. 1,2 The vector of research in QCLs has shifted toward frequency comb regimes through four-wave mixing in the gain medium, with predominantly frequency-modulated output. 3-5

In interband diode lasers the situation is much more favorable for passive mode-locking, since the interband recombination time is typically on the order of 1 ns, i.e., much longer than the cavity round-trip time. Intracavity saturable absorption needed for pulse formation can be implemented by keeping a short section of the cavity under reverse bias. Passively mode-locked semiconductor lasers were shown to generate intensive ps-scale pulses with tens of GHz repetition rates and achieve the highest level of integration.⁶ Although the overwhelming majority of diode lasers operate in the near-infrared and visible spectral ranges, GaSb-based type-I quantum well cascade diode laser technology covers a spectral region from below 2 to over 3 μ m, offering access to absorption features of a variety of technologically important gases as well as atmospheric transparency windows. The optical frequency combs generated by these devices can be used in the compact dual-comb spectroscopic sensors.8 Passive mode-locking of the noncascade type-I quantum well GaSbbased diode lasers operating near 2 µm was reported in refs 9 and 10, where optical and radio frequency (RF) spectral characteristics of the corresponding two-section split-contact devices were described. The devices demonstrated the intermodal beat notes with Lorentzian line width in the range of tens of kHz. The mode-locked operation of these devices was achieved when reverse bias was applied to the absorber section to minimize its recovery time. In the splitcontact 3.6 µm interband cascade lasers (ICLs) with type-II quantum well (QW) active region the saturable absorber recovery time was reduced by ion implantation, i.e., without reverse bias. 11 The ICLs demonstrated narrow sub-kHz intermodal beat notes, permitting multiheterodyne spectroscopy near 3.2 μ m. ¹² In the interband lasers, the spontaneous emission phase noise can contribute to coherence degradation reflected in the increased intermodal beat note line width. 13 It was argued that a certain degree of optical phase-locking induced by four-wave-mixing (as observed in intersubband quantum cascade lasers⁴) can be present in ICLs and explain relatively narrow beat notes in the corresponding passively mode-locked devices. The phase-locking efficiency is often limited by the group velocity dispersion (GVD). 14 The laser heterostructure optimization can help to minimize the coupling of the spontaneous emission to laser mode as well as to control the waveguide GVD to improve the coherence of the interband mode-locked lasers. The analysis of the effect of the reverse bias on the absorber section of the cascade laser

Received: August 30, 2018 Published: November 21, 2018

[†]Stony Brook University, Stony Brook, New York 11794, United States

[‡]Texas A&M University, College Station, Texas 77843, United States

heterostructures deserves special attention. In regular diode lasers the reverse bias helps to extract photoexcited carriers from absorber QWs by means of the field-assisted thermionic emission. In cascade laser structures the active QWs are surrounded by carrier injectors often made of superlattices (SLs) designed to form resonant minibands under forward bias condition. Under reverse bias these SL structures might not necessarily be able to provide efficient carrier extraction. As discussed further, the peculiarity of the hole injector design of GaSb-based type-I QW cascade diode lasers permits efficient hole extraction under reverse bias conditions.

In this work we report on the first demonstration of passive mode-locking of GaSb-based type-I QW cascade diode lasers. The devices utilize a split-contact narrow ridge design. Lasers with a reverse-biased absorber section generate ~10 ps pulses with above 10 mW peak power at the repetition frequency of \sim 13.2 GHz. The devices operate near 3.25 μ m, covering a spectral region of more than 20 nm with its frequency comb spectrum. A stable intermodal beat note with a 180 kHz Lorentzian line width was observed. The two-photon absorption (TPA) interferometric autocorrelation (IAC) studies showed that the devices generated chirped pulses with a duration of about 3 times more than the transform limit. A small degree of optical phase-locking was observed in autocorrelation traces even when both gain and absorber sections were forward biased, i.e., when the device worked almost as a single-section Fabry-Perot laser. Self-mode-locking without an absorber section was demonstrated in quantum dash,16 quantum dot,17 and quantum cascade lasers,3-5,18 contributed by fast carrier lifetime, engineered GVD, and/or nonlinear four-wave mixing.

LASER HETEROSTRUCTURE DESIGN AND DEVICE FABRICATION

Three-stage cascade diode laser heterostructures were grown by solid-source molecular beam epitaxy on Te-doped GaSb substrates. Each cascade contained 13-nm-wide ~1.5% compressively strained GaInAsSb QWs with a nominal indium composition of 58% and generating optical gain peaking near 3.2 μ m at room temperature. The 2.2- and 2- μ m-thick n- and p-cladding layers were made of AlGaAsSb quaternary alloy with 80% aluminum content. The waveguide core was formed by a ~300-nm-thick GaSb layer between the n-clad and the active region and ~350 nm of AlGaInAsSb (with ~30% aluminum and indium contents) between the active region and the p-cladding. The InAs/AlSb SL between GaSb and the QW in the first cascade was added to confine the holes. The compositionally graded AlGaAsSb (aluminum content changed from 50% down to 5% over 100 nm) layers and chirped InAs/ AlSb SL layers realized a series connection of the three active QWs, i.e., a cascade pumping scheme. The top part of Figure 1 shows the schematic energy band diagram. This structure was previously used to fabricate the anti/high-reflection coated 100- μ m-wide ridge multimode and \sim 9.5- μ m-wide ridge single spatial mode 3.25 µm lasers generating 350 and 50 mW of continuous wave (CW) output power,7 respectively, when soldered epi-side-down to a heatsink kept at 20 °C. Figure 2 shows the simulated band diagram of the central cascade under forward and reverse bias conditions. The forward bias (Figure 2a) case illustrated the standard operation (~0.7 V per cascade) of the laser heterostructure when electrons and holes are delivered to active QWs to generate optical gain. The large overlap between electron and hole wave functions in 13-nm-

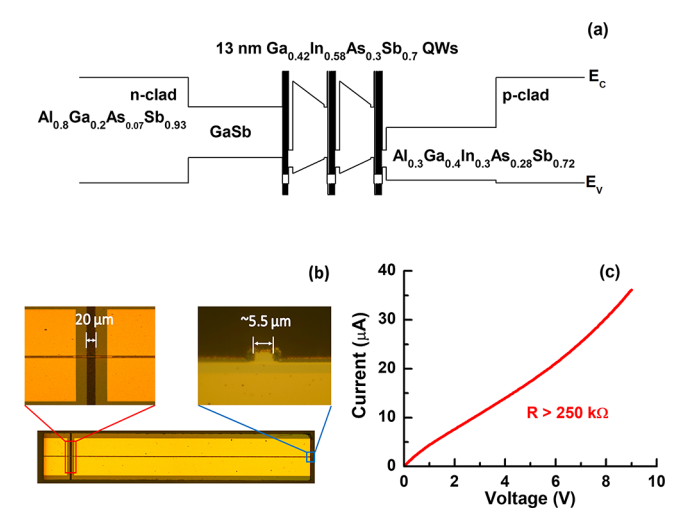


Figure 1. (a) Schematic band diagram of the three-stage cascade type-I QW diode laser heterostructure under flat band condition. (b) Top view optical image of the split-contact narrow ridge lasers. Insets show the magnified images of the top view of the etched trench between absorber and gain sections and the cross-section of the laser NR coated facet. (c) Current—voltage characteristics measured when the absorber section was negatively biased with respect to the gain section.

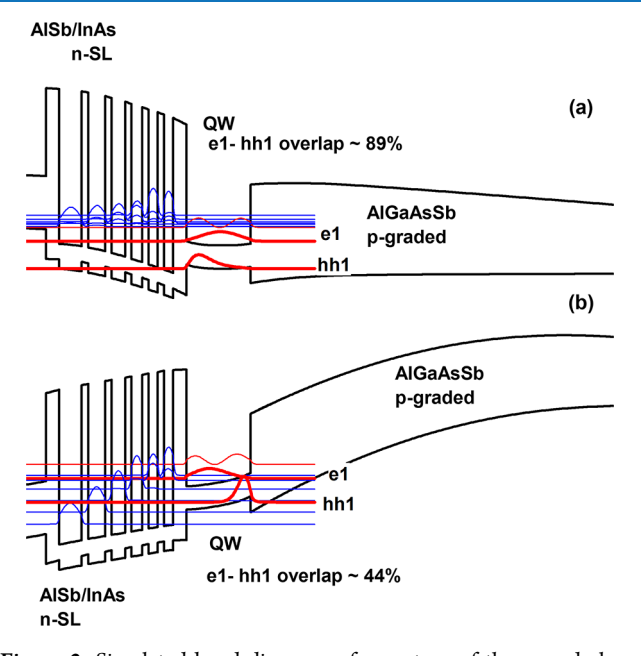


Figure 2. Simulated band diagrams of one stage of the cascade laser heterostructure under (a) forward bias of 0.7 V/stage and (b) reverse bias of -2 V/stage.

wide QWs helps to minimize the laser threshold current (below 250 A/cm² was reported for benchmark 100- μ m-wide ridge multimode devices). The InAs/AlSb electron injector forms a miniband for electron transport from the GaSb/AlSb/InAs tunnel junction to active QWs. The holes are delivered by drift-diffusion through the graded bandgap layer.

Under reverse bias (-2 V per cascade, Figure 2b) the electron injector is misaligned and electrons photoexcited in active QWs can escape through a ladder of electron states by phonon scattering. The holes can be extracted like in standard noncascade type-I QW biased absorbers, i.e., by field-assisted thermionic emission. Thus, escaped holes are delivered to

either tunnel junction interface, where they recombine with electrons (in the first and second cascades as counted from the left in Figure 1a) or directly to p-cladding (in the last stage).

Arguably, the hole extraction can be the mechanism limiting the reduction of the absorber recovery time under reverse bias condition. The electron extraction to the superlattice injector and Auger-assisted recombination at the ultralow bandgap GaSb/InAs interface having a large number of electrons can be rather fast.

The cascade diode laser heterostructure was processed into \sim 5.5- μ m-wide ridges using chlorine-based reactive ion etching (left inset in Figure 1b). The ridges were etched through the top p-cladding and the active region (etching depth $\sim 3 \mu m$). Devices with a $\sim 300 - \mu \text{m}$ -long absorber section and a 2.7-mmlong gain section were fabricated. The electrical isolation between gain and absorber sections of the split-contact devices was enforced by etching an additional ~ 20 - μ m-wide and ~ 1.5 - μ m-deep trench (right inset in Figure 1b). The resistance between the gain and absorber sections was measured to be >250 k Ω , which implies less than 40 μ A of the crosstalk current at the maximum absorber-to-gain section bias of ~9 V (Figure 1c). The lasers were neutral-reflection (NR) (~32%) and high-reflection (HR) (~98%) coated on gain and absorber section facets, respectively. The devices were indium soldered epi-side-up onto gold-plated copper blocks, which were bolted to a temperature-stabilized heatsink.

EXPERIMENTAL METHODS

Device average output power was measured by a large-area calibrated thermopile photodetector. The current and voltage biases were obtained from an Agilent E3631A DC power supply. The operating voltage was measured by a Keithley 6517 electrometer. The device output spectra were characterized by a Nicolet 6700 Fourier transform infrared spectrometer equipped with an external liquid nitrogen cooled InSb photodetector (Teledyne J10D) and using a CaF₂ beam splitter. Laser modal gain spectra were measured using the Hakki–Paoli method.

The AC component of the absorber section voltage signal was fed through bias-T (Picosecond Pulse Lab, 40 GHz bandwidth) to the Agilent 83006A preamplifier (26.5 GHz bandwidth). Thus, the collected RF spectrum was measured by an HP 8592L electrical spectrum analyzer (22 GHz bandwidth) to characterize intermodal beat note parameters.

Second-order IAC measurements were performed using a Michelson interferometer with a pellicle beam splitter and gold-plated retroreflectors. The delay line was controlled by a motorized micrometer with a resolution of ~35 nm. The TPA signal was collected by a small-area InGaAs photodetector (JDSU ETX 75TL, 75 μ m diameter and 1.7 μ m cutoff) with a germanium filter (2.3 μ m cutoff) and a Stanford Research SR 570 amplifier.

EXPERIMENTAL RESULTS AND DISCUSSION

Figure 3 shows the device light-current—voltage characteristics measured in the CW regime at 20 °C. When both gain and absorber sections were forward biased, the lasers demonstrated a threshold current of about 100 mA and generated above 10 mW at 400 mA, corresponding to a voltage drop of about 2.4 V. The single lobe current independent lateral far field pattern (inset in Figure 3) corresponded to stable single spatial mode operation of the deep etched ridge lasers. When the absorber

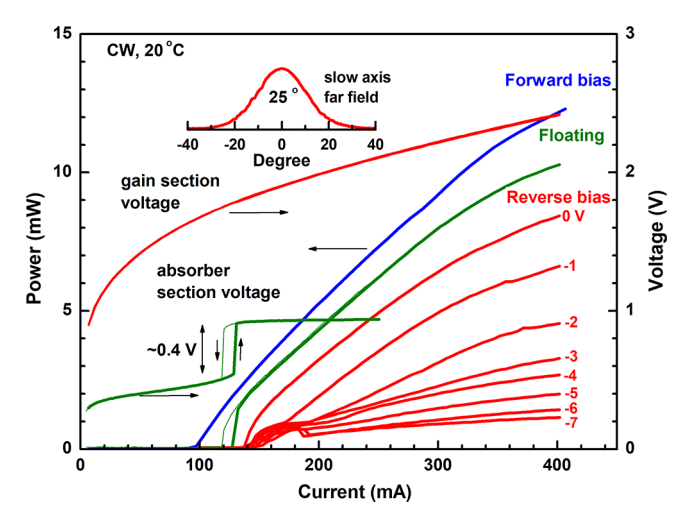


Figure 3. CW light-current—voltage characteristics measured at 20 $^{\circ}$ C for epi-side-up mounted NR/HR coated lasers with 2.7 mm long gain and 0.3 mm long absorber sections. The absorber bias conditions were varied from forward to reverse. The inset shows the measured slow axis far-field pattern. The voltage drop across the gain section is shown for floating and reverse-biased absorber section conditions. The voltage drop across the absorber section is shown for the floating absorber case. The voltage—current and power—current characteristics corresponding to an increase (thick line) and decrease (thin line) of the current under conditions of the floating absorber demonstrate apparent hysteresis behavior.

section was left floating and only the gain section was forward biased, the threshold increased and efficiency decreased. The devices with a floating absorber demonstrated bistable light-current—voltage characteristics with apparent hysteresis. The abrupt increase of the output power is associated with optical bleaching of the absorber section, hence reduction of the cavity round-trip loss. Different values of the laser thresholds under increased and decreased the gain section currents were observed due to the presence of a large number of intracavity photons in the latter case. A similar hysteresis phenomenon has been observed in other types of passively mode-locked semiconductor lasers; see for instance ref 20. The voltage drops across the floating absorber section increased by ~ 0.4 V after the lasing started, indicative of the quasi-Fermi level separation increase with intensity of the photoexcitation.

The laser threshold current further increased when voltage drop across the absorber section was set at 0 V. Application of the reverse bias of up to -7 V to the absorber section almost did not increase the device threshold current any further but led to gradual reduction of the laser average output power. Figure 4 shows the laser emission spectra at different bias conditions. When the absorber section was forward biased or left floating, the laser spectra demonstrated an irregular shape with a modulation period of ~5 nm, corresponding to the presence of the ~300-µm-long intracavity etalon associated with the absorber section. Figure 4a shows that when both the gain section and absorber section were forward biased, the laser spectra demonstrated an usual thermal red shift accompanied by broadening. At the higher currents (starting from about twice the threshold), the laser spectra split into two bands. The separation between the bands increases with the laser power (Figure 4b).

Although the bands are too broad to make any definite conclusion about functional dependence of the splitting energy on laser power, this behavior bears a striking similarity to the

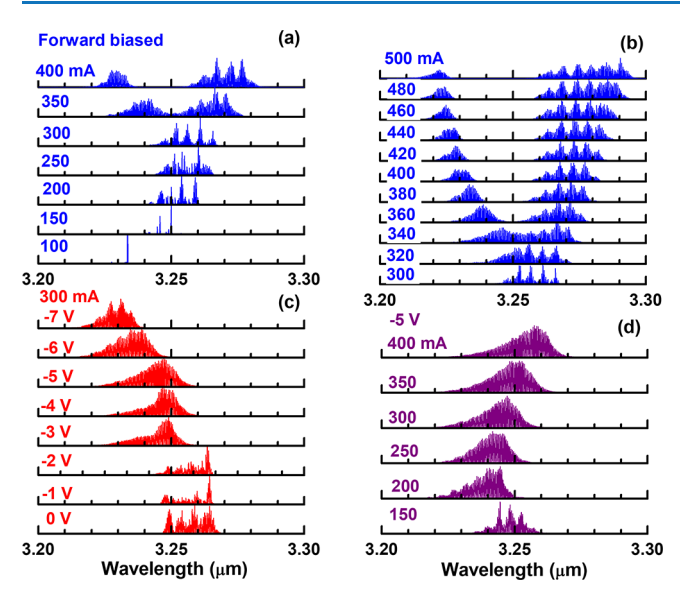


Figure 4. Laser emission spectra measured (a and b) at different currents above threshold and when both absorber and gain section were forward biased; (c) at a gain section current of 300 mA with different reverse biases on the absorber section ranging from 0 to -7 V; (d) at -5 V reverse bias applied to the absorber section and different gain section currents ranging from 150 to 400 mA.

coherent multimode instability observed in mid-infrared QCLs,²¹ named RNGH instability after the initials of the authors who predicted it in the late 1960s: Risken and Nummedal²² and independently Graham and Haken.²³ The origin of this phenomenon is the coherent oscillations of the population inversion at the Rabi frequency, which takes place when the intracavity laser intensity becomes sufficiently large. This results in a parametric nonlinear deformation of the gain spectrum and the emergence of sidebands separated from the maximum of the small-signal gain curve by an amount corresponding to the Rabi frequency, i.e., proportional to the square root of the laser power. In QCLs the multimode generation is attributed mainly to the interplay between the incoherent mechanism of spatial hole burning, which leads to a proliferation of modes with uncorrelated phases, and the coherent RNGH-type mechanism.²⁴ In the interband diode lasers, spatial hole burning effects may be suppressed by carrier diffusion; instead, it is the spectral hole burning due to inhomogeneous broadening of interband transitions that can become important in multimode generation and lowering the threshold for coherent instabilities.2

Figure 4c shows the dependence of the laser emission spectra on absorber bias at a fixed gain section current of 300 mA. Starting from absorber bias voltages of about -3 V, the laser spectra got smoothed and started assuming a bell-curve-like shape. The smoothing of the laser spectra with increasing absorber bias was accompanied by a slight blue shift. The blue shift can be caused by bandgap reduction due to the Stark effect in the QW of the reverse-biased absorber section, leading to an increase of the optical loss in the long-wavelength part of the spectrum. Figure 4d shows the dependence of the laser spectra on current for a fixed absorber reverse bias of -5 V. The smooth optical frequency comb spectra were observed starting from about 200 mA of the gain section current. The thermal red shift was apparent with further current increase.

Figure 5a shows the modal gain spectra measured at several underthreshold currents when both the gain and the absorber

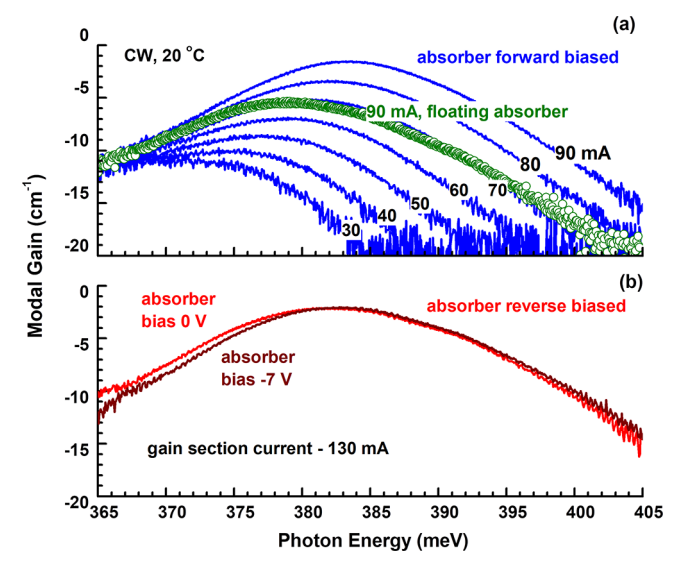


Figure 5. (a) Modal gain spectra measured for several underthreshold currents for the device with both gain and absorber sections forward biased (lines). The gain spectrum measured at 90 mA of the gain section current and floating absorber is shown in open circles. (b) Modal gain spectra measured at 0 and -7 V of reverse bias voltage applied to the absorber section and at the gain section current of 130 mA (close to threshold).

sections were forward biased (solid lines). The internal optical loss of ${\sim}10~\text{cm}^{-1}$ can be estimated from the long-wavelength part of the modal gain spectra (distributed mirror loss was estimated as ${\sim}2~\text{cm}^{-1}$ for ${\sim}3\text{-mm}\text{-long NR/HR}$ coated lasers). The transparency was achieved at a current of ${\sim}30~\text{mA}$. The device started lasing at a CW current just above 90 mA at 20 $^{\circ}\text{C}$.

When the absorber section was disconnected from the power supply while the same ~90 mA was flowing through the gain section, the modal gain peak value dropped by ~4 cm⁻¹ (open circles in Figure 5a). The extra loss introduced by the unpumped absorber section can be compensated by an increase of the current through the gain section up to \sim 130 mA. The further application of the reverse bias to the absorber section up to -7 V had a moderate effect on the underthreshold device modal gain spectra (Figure 5b). Small blue shift of the modal gain long-wavelength edge was observed, which can be ascribed to a Stark red shift of the active QW absorption edge in the electric field. This slight blue shift of the gain peak corresponds to the observed blue shift of the laser emission with increasing the absorber section bias (Figure 4c). We speculate that the application of the reverse bias to the absorber section mostly affects the absorber recovery time but not its saturable loss value.

The clear intermodal beat note was observed for gain section currents ranging from 100 to 400 mA at absorber section bias voltages varied from 0 to -7 V. Figure 6a plots the map of the RF spectrum of the absorber voltage at the absorber bias of -6.5 V. Figure 6b shows a high-resolution scan (3 kHz) corresponding to 300 mA of the gain section current. The operation conditions—300 mA of gain section current and -6.5 V of absorber bias voltage—fall into the region of parameters corresponding to the narrowest Lorentzian line width of the intermodal beat note. The line width of about 180 kHz peaking near 13.25 GHz was observed. The effective group refractive index estimated from the RF beat note peak

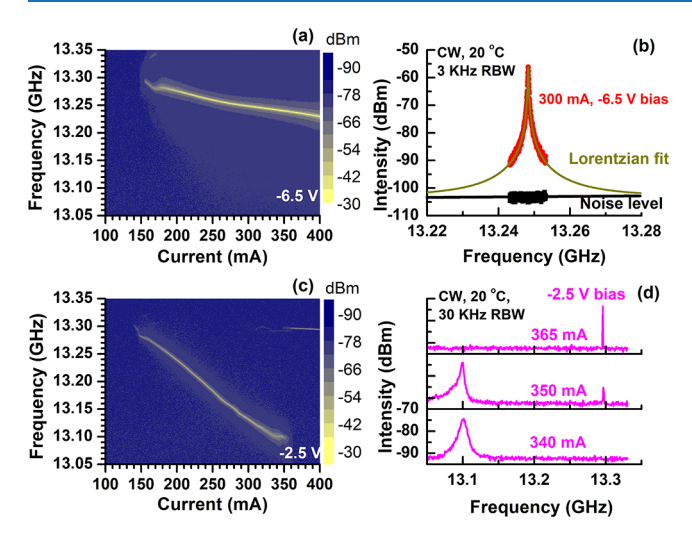


Figure 6. (a and c) RF intensity maps (in dB scale) taken over a gain section current range from 100 to 400 mA and for -6.5 V (a) and -2.5 V (c) of the reverse bias on the absorber. (b) High-resolution intermodal beat note measured at a gain section current of 300 mA and absorber section bias of -6.5 V. Lorentzian fit and noise floor are also shown. (d) Low-resolution RF spectra measured at -2.5 V of the absorber section bias and different gain section currents.

frequency was about 3.77, matching the estimation of the refractive index from the free spectral range in the laser emission spectra (Figure 4).

The transition between bistable mode-locking regimes was observed at lower absorber section biases. For instance, at an absorber section bias of -2.5 V, the dominant RF beat note frequency abruptly changed from ~ 13.1 GHz to ~ 13.3 GHz when the gain section current was increased above 350 mA (Figure 6c and d). The strong phase-amplitude coupling in the gain and absorber sections was invoked to model this complex dynamical behavior of semiconductor lasers. ²⁶ Notably, the Lorentzian line width of the RF beat note decreased dramatically (from above 5 MHz to ~ 30 kHz) on transition to the second mode-locking branch with increasing the pumping level of the gain section.

Figure 7 plots the intermodal beat note frequency and its Lorentzian line width in the first mode-locking branch as a

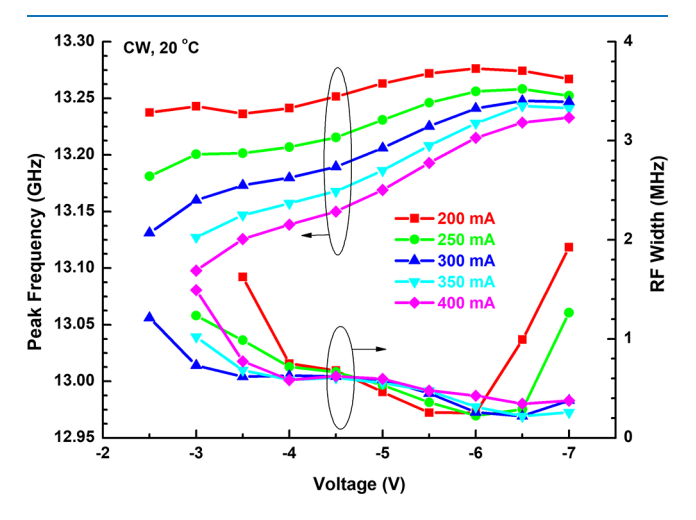


Figure 7. Peak frequency and Lorentzian width of the intermodal beat note measured for different gain section currents and absorber section reverse bias voltages.

function of the gain section pumping current and absorber bias voltage. Increase of the gain section current leads to reduction of the intermodal beat note frequency presumably due to the increase of group index with gain. This effect tends to weaken with an increase of the absorber section bias. The beat note Lorentzian line width decreases with the absorber section bias, reaching a relatively flat minimum. The observed intermodal beat note line width below 200 kHz corresponds to the pulseto-pulse timing jitter of about 110 fs/cycle, calculated based on ref 27. The somewhat excessive noise can be associated with the strong contribution of the spontaneous emission to the laser mode, which can be addressed by redesign of the laser waveguide structure targeting the reduced active region optical confinement factor and dispersion compensation. This optimization as well as a quantitative understanding of the RF beat note dynamics requires detailed modeling that is outside the scope of this first demonstration effort.

Temporal pulse characteristics were studied using secondorder IAC measurements. The autocorrelation measured for the case when both gain and absorber sections were forward biased is shown in Figure 8a (bottom curve). The presence of

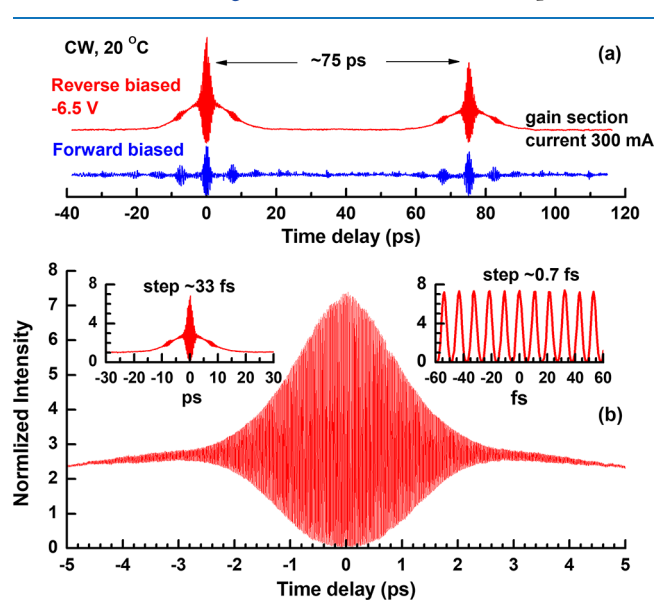


Figure 8. (a) Two-photon IAC traces measured at 300 mA of the gain section current for the cases of forward biased and the -6.5 V reverse-biased absorber section. (b) High-resolution IAC measured near the zero delay for 300 mA of gain section current and -6.5 V of the absorber section reverse bias. Left inset is the corresponding low-resolution IAC trace measured in a wider range of time delays. Right inset is a magnified section of the high-resolution IAC in the vicinity of the zero time delay.

the apparent autocorrelation bands separated by cavity round-trip time (\sim 75 ps) indicates a certain degree of phase-locking between laser modes even without any saturable absorber action. This could be caused by the third-order nonlinearity. This is a weak effect in interband diode lasers, and its ability to provide efficient phase-locking between modes is limited by cavity dispersion and carrier diffusion. Arguably, this phenomenon can contribute to the observed instability at low absorber bias levels (Figure 6c and d) when cavity dispersion can be somewhat minimized by gain flattening at high pumping levels. Similar autocorrelation traces indicating a small degree of amplitude or frequency modulation were

observed at absorber bias voltages up to ~ -2 V. When absorber section bias was increased above -2 V, the IAC scans corresponded to a clear pulse train (top curve in Figure 8a corresponds to an absorber bias of -6.5 V). Figure 8b plots a high-resolution IAC scan (100 nm delay line step corresponding to ~ 0.7 fs time delay step) near zero delay at -6.5 V of absorber bias and 300 mA of the gain section current. Insets to Figure 8b show the wider delay range scan with ~33 fs time step (left) and magnified section of the IAC near zero delay (right). The peak-to-background ratio was approaching 8:1, which is an expected value for interferometric autocorrelation of the coherent pulsed emitter.²⁸ The pedestal around the interferometric fringes indicates the presence of a strong chirp in the pulse and serves as a natural way of observing intensity autocorrelation also characterized by a classic 3:1 peak-tobackground intensity ratio. The interferometric fringe separation of about 10.9 fs (right inset to Figure 8b) corresponds to the laser operating wavelength of $\sim 3.25 \mu m$.

Figure 9a shows the collection of IAC traces measured near zero delay when a current of 300 mA was flowing through the

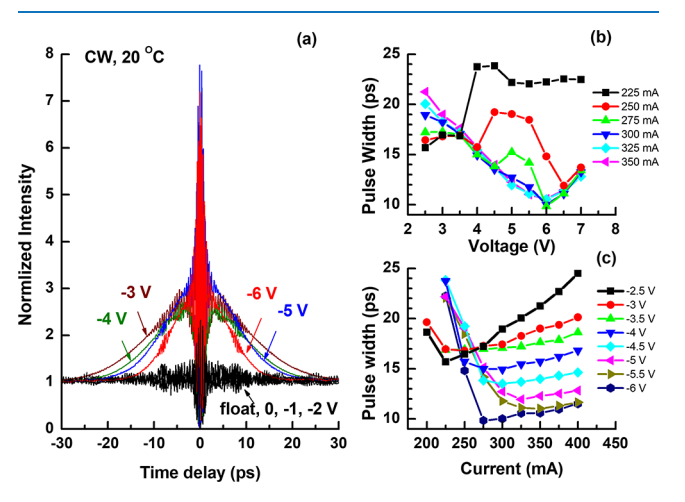


Figure 9. (a) IAC traces measured with 300 mA of gain section current for variable absorber section reverse bias voltages ranging from -2 to -6 V. (b and c) Dependences of the pulse width estimated form IAC on gain section current and absorber section reverse bias voltage.

gain section and absorber bias voltage was varied from 0 to -6 V. Once the bias section voltage was increased above -2 V, we observed a strong increase of the intensity at zero delay. Figure 9b and c plot the dependence of the chirped pulse width estimated from the width of the IAC scans as a function of the absorber bias at different gain section currents. The pulse width tends to decrease with the absorber bias from ~ 20 ps at -3 V down to ~ 10 ps at -6 V. Further increase of the absorber bias to -7 V led to pulse broadening.

At a fixed absorber section bias of -5 V the high-contrast IAC traces were observed starting from \sim 250 mA of the gain section current. The current increase up to 300 mA led to apparent pulse narrowing down to \sim 10 ps, while further current increases up to 400 mA increased the pulse width slightly. The comparison of the thus estimated pulse duration with the measured laser spectrum (Figure 4) allows concluding that the first generation of the GaSb-based cascade diode passive mode-locked lasers generate strongly chirped pulses that are about 3 times longer than the transform limit.

The confirmation of the laser short pulse operation and a rough estimation of the pulse width can be obtained without autocorrelation studies by simple comparison of the average signals in one-photon and two-photon detection regimes. Under rough approximation of the rectangular pulse shape, the ratio of one-photon detector signals for mode-locked and CW device operations can be expressed as

$$A = \frac{P_{\text{peal}} f_{\text{RF}} \Delta t}{P_{\text{CW}}} \tag{1}$$

where $P_{\rm peak}$ and $P_{\rm CW}$ are peak and CW values of the laser power in mode-locked and CW regimes, respectively. The $f_{\rm RF}$ and Δt are pulse train repetition frequency and pulse width, respectively.

In the two-photon detection regime the detector signal ratio will be

$$B = \frac{P_{\text{peak}}^2 f_{\text{RF}} \Delta t}{P_{\text{CW}}^2} \tag{2}$$

Thus, the pulse width can be expressed as

$$\Delta t = \frac{A^2}{B} \frac{1}{f_{\rm RF}} \tag{3}$$

Figure 10a shows the time average light-current characteristics measured by an InGaAs photodetector (two-photon

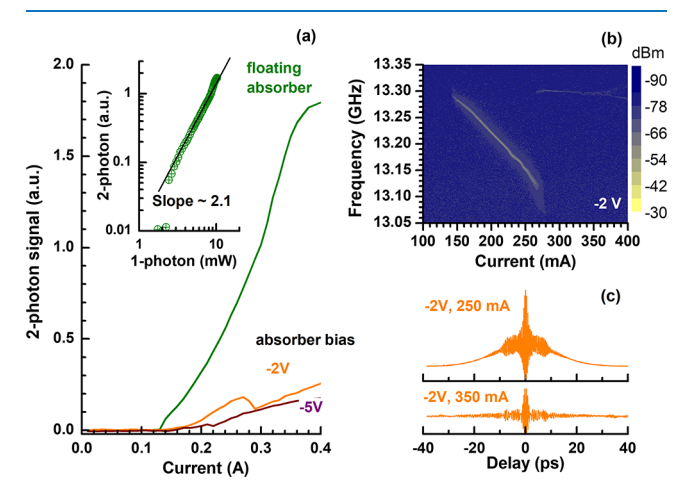


Figure 10. (a) Current dependence of the two-photon signal for the cases of floating and biased (-2 and -5 V) absorber section. Inset shows the dependence of the two-photon signal on laser output power measured for the case of the floating absorber section. (b) RF intensity map (in dB scale) measured over a range of gain section currents from 100 to 400 mA for -2 V of absorber section reverse bias. (c) IAC traces measured at gain section currents of 250 and 350 mA with -2 V of the absorber section reverse bias.

detection regime) for the floating and the -2 and -5 V biased absorber sections. The inset shows the dependence of the two-photon detector signal on laser power measured in the one-photon detection regime (Figure 3) for the device with a floating absorber. The slope of ~ 2 in double-logarithmic scale confirms two-photon detection by the InGaAs photodetector.

The ratios A and B from eqs 1 and 2 found for the absorber section bias of -5 V and gain section current of 300 mA can be used for a rough estimation of the pulse width yielding $\Delta t \approx 20$ ps. At the absorber bias of -2 V, an abrupt transition between two RF beat note frequencies was observed at a current of

about 275 mA (Figure 10b). The pulse width below and above the transition point can be estimated as ~33 and ~114 ps. The latter value exceeds the round-trip frequency and thus does not make physical sense. One can conclude that the pulse disappears at high currents with small absorber section bias. Figure 10c shows the autocorrelation scans measured at the currents corresponding to below and above RF beat note frequency jump. At lower current the autocorrelation trace indicates the presence of the chirped pulse and shows adequate peak-to-background contrast. At high current the autocorrelation scan indicated only minor amplitude or frequency modulation.

CONCLUSION

We report on the first demonstration and comprehensive characterization of passively mode-locked GaSb-based type-I quantum well cascade diode lasers. The devices operated near 3.25 μ m and utilized split-contact architecture. When both absorber and gain sections were connected in parallel, the lasers operated in the continuous wave regime with irregular emission spectra. At increased pumping levels the laser emission spectra split into two bands with the powerdependent splitting energy. This effect was similar to the coherent multimode RNGH instability observed in midinfrared QCLs. The devices with a reverse-biased absorber section generated ~10 ps pulses at the repetition rate of ~13 GHz with average power exceeding 1 mW. The laser emission spectrum in the mode-locked regime comprised a smooth bellshape-like frequency comb covering about a 20 nm range at full-width at half-maximum level. Interferometric autocorrelation studies revealed a strong spectral chirp in the pulses. The intermodal beat note with the minimum Lorentzian line width of 180 kHz was observed at -6.5 V of absorber reverse bias. A small degree of the phase-locking was detected in autocorrelation scans even when both gain and absorber sections were forward biased, i.e., when both absorber and gain sections were connected in parallel. The mapping of the radio frequency spectrum over variable gain and absorber section biases showed switching between two bistable mode-locking regimes at low absorber bias section voltages. A simple method of estimation of the pulse width of the mode-locked lasers was proposed. The method is based on comparison of the average signals in single- and two-photon detection regimes.

AUTHOR INFORMATION

Corresponding Author

*E-mail: leon.shterengas@stonybrook.edu.

ORCID ®

Leon Shterengas: 0000-0002-8563-3274

Notes

The authors declare no competing financial interest.

ACKNOWLEDGMENTS

The work was supported by the U.S. National Science Foundation, grant ECCS-1707317. One of the authors (T.F.) would like to acknowledge China Scholarship Council for the financial support. The authors would like to thank the G. Belenky, M. Bagheri, and J. R. Meyer for fruitful discussions.

REFERENCES

(1) Wang, C. Y.; Kuznetsova, L.; Gkortsas, V. M.; Diehl, L.; Kärtner, F. X.; Belkin, M. A.; Belyanin, A.; Li, X.; Ham, D.; Schneider, H.;

Grant, P.; Song, C. Y.; Haffouz, S.; Wasilewski, Z. R.; Liu, H. C.; Capasso, F. Mode-locked pulses from mid-infrared quantum-cascade lasers. *Opt. Express* **2009**, *17*, 12929.

- (2) Revin, D. G.; Hemingway, M.; Wang, Y.; Cockburn, J. W.; Belyanin, A. Active mode locking of quantum cascade lasers operating in external ring cavity. *Nat. Commun.* **2016**, *7*, 11440.
- (3) Yu, N.; Diehl, L.; Cubukcu, E.; Bour, D.; Corzine, S.; Höfler, G.; Wojcik, A. K.; Crozier, K. B.; Belyanin, A.; Capasso, F. Coherent Coupling of Multiple Transverse Modes in a Quantum Cascade Laser. *Phys. Rev. Lett.* **2009**, *102*, 013901.
- (4) Hugi, A.; Villares, G.; Blaser, S.; Liu, H. C.; Faist, J. Mid-infrared frequency comb based on a quantum cascade laser. *Nature* **2012**, *492*, 229.
- (5) Kazakov, D.; Piccardo, M.; Wang, Y.; Chevalier, P.; Mansuripur, T. S.; Zah, C.; Lascola, K.; Belyanin, A.; Capasso, F. Self-starting harmonic frequency comb generation in a quantum cascade laser. *Nat. Photonics* **2017**, *11*, 789.
- (6) Keller, U. Recent developments in compact ultrafast lasers. *Nature* **2003**, 424, 831–838.
- (7) Shterengas, L.; Kipshidze, G.; Hosoda, T.; Liang, R.; Feng, T.; Wang, M.; Stein, A.; Belenky, G. Cascade Pumping of 1.9–3.3 μm Type-I Quantum Well GaSb-Based Diode Lasers. *IEEE J. Sel. Top. Quantum Electron.* **2017**, 23, 16921011.
- (8) Schliesser, A.; Picqué, N.; Hänsch, T. W. Mid-infrared frequency combs. *Nat. Photonics* **2012**, *6*, 440–449.
- (9) Merghem, K.; Teissier, R.; Aubin, G.; Monakhov, A. M.; Ramdane, A.; Baranov, A. N. Passive mode locking of a GaSb-based quantum well diode laser emitting at 2.1 μ m. Appl. Phys. Lett. **2015**, 107, 111109.
- (10) Li, X.; Wang, H.; Qiao, Z.; Guo, X.; Ng, G. I.; Zhang, Y.; Niu, Z.; Tong, C.; Liu, C. Modal gain characteristics of a 2 μ m InGaSb/AlGaAsSb passively mode-locked quantum well laser. *Appl. Phys. Lett.* **2017**, *111*, 251105.
- (11) Bagheri, M.; Frez, C.; Sterczewski, L. A.; Gruidin, I.; Fradet, M.; Vurgaftman, I.; Canedy, C. L.; Bewley, W. W.; Merritt, C. D.; Kim, C. S.; Kim, M.; Meyer, J. R. Passively mode-locked interband cascade optical frequency combs. *Sci. Rep.* **2018**, *8*, 3322.
- (12) Sterczewski, L. A.; Westberg, J.; Patrick, C. L.; Kim, C. S.; Kim, M.; Canedy, C. L.; Bewley, W. W.; Merritt, C. D.; Vurgaftman, I.; Meyer, J. R.; Wysocki, G. Multi-heterodyne spectroscopy using interband cascade lasers. *Opt. Eng.* **2018**, *57*, 011014.
- (13) Kim, I.; Lau, K. Y. Frequency and timing stability of mode-locked semiconductor lasers-passive and active mode locking up to millimeter wave frequencies. *IEEE J. Quantum Electron.* **1993**, 29, 1081
- (14) Faist, J.; Villares, G.; Scalari, G.; Rösch, M.; Bonzon, C.; Hugi, A.; Beck, M. Quantum Cascade Laser Frequency Combs. *Nanophotonics* **2016**, *5* (2), 272.
- (15) Malins, D. B.; Gomez-Iglesias, A.; White, S. J.; Sibbett, W.; Miller, A.; Rafailov, E. U. Ultrafast electro absorption dynamics in an InAs quantum dot saturable absorber at 1.3 μ m. Appl. Phys. Lett. **2006**, 89, 171111.
- (16) Gosset, C.; Merghem, K.; Martinez, A.; Moreau, G.; Patriarche, G.; Aubin, G.; Ramdane, A.; Landreau, J.; Lelarge, F. Subpicosecond pulse generation at using a quantum-dash-based Fabry-Perot laser emitting at $1.56~\mu m$. *Appl. Phys. Lett.* **2006**, 88, 241105.
- (17) Liu, J.; Lu, Z.; Raymond, S.; Poole, P. J.; Barrios, P. J.; Poitras, D. Dual-wavelength 92.5 GHz self-mode-locked InP-based quantum dot laser. *Opt. Lett.* **2008**, 33 (15), 1702–1704.
- (18) Lu, Q. Y.; Razeghi, M.; Slivken, S.; Bandyopadhyay, N.; Bai, Y.; Zhou, W. J.; Chen, M.; Heydari, D.; Haddadi, A.; McClintock, R.; Amanti, M.; Sirtori, C. High power frequency comb based on midinfrared quantum cascade laser at $\lambda \sim 9~\mu m$. *Appl. Phys. Lett.* **2015**, 106, 051105.
- (19) Hakki, B. W.; Paoli, T. L. Gain spectra in GaAs double-heterojunction injection lasers. *J. Appl. Phys.* **1975**, *46*, 1299.
- (20) Xiaodong, H.; Stintz, A.; Hua, L.; Rice, A.; Liu, G. T.; Lester, L. P.; Cheng, J.; Malloy, M. J. Bistable operation of a two-section 1.3 μ m

InAs quantum dot laser-absorption saturation and the quantum confined Stark effect. *IEEE J. Quantum Electron.* **2001**, 37, 414.

- (21) Gordon, A.; Wang, C. Y.; Diehl, L.; Kärtner, F. X.; Belyanin, A.; Bour, D.; Corzine, S.; Höfler, G.; Liu, H. C.; Schneider, H.; Maier, T.; Troccoli, M.; Faist, J.; Capasso, F. Multimode regimes in quantum cascade lasers: From coherent instabilities to spatial hole burning. *Phys. Rev. A: At., Mol., Opt. Phys.* **2008**, *77*, 053804.
- (22) Risken, H.; Nummedal, K. Self-pulsing in lasers. J. Appl. Phys. 1968, 39, 4662.
- (23) Graham, R.; Haken, H. Quantum theory of light propagation in a fluctuating laser-active medium. Z. Phys. A: Hadrons Nucl. 1968, 213, 420.
- (24) Mansuripur, T. S.; Vernet, C.; Chevalier, P.; Aoust, G.; Schwarz, B.; Xie, F.; Caneau, C.; Lascola, K.; Zah, C.; Caffey, D. P.; Day, T.; Missagia, L. J.; Connors, M. K.; Wang, C.; Belyanin, A.; Capasso, F. Single-mode instability in standing-wave lasers: quantum cascade laser as a self-pumped parametric oscillator. *Phys. Rev. A: At., Mol., Opt. Phys.* **2016**, *94*, 063807.
- (25) Khanin, Y. I. Principles of Laser Dynamics; Elsevier: Amsterdam,
- (26) Pimenov, A.; Habruseva, T.; Rachinskii, D.; Hegarty, S. P.; Huyet, G.; Vladimirov, A. G. Effect of dynamical instability on timing jitter in passively mode-locked quantum-dot lasers. *Opt. Lett.* **2014**, 39, 24.
- (27) Kefelian, F.; O'Donoghue, S.; Todaro, M. T.; McInerney, J. G.; Huyet, G. RF Linewidth in Monolithic Passively Mode-Locked Semiconductor Laser. *IEEE Photonics Technol. Lett.* **2008**, 20, 1405.
- (28) Weiner, A. M. Ultrafast Optics; Wiley, 2009.